Strongly enhanced photon collection from diamond defect centers under microfabricated integrated solid immersion lenses

J. P. Hadden, J. P. Harrison, A. C. Stanley-Clarke, L. Marseglia, Y.-L. D. Ho, B. R. Patton, J. L. O'Brien, and J. G. Rarity

View Online   Export Citation

ARTICLES YOU MAY BE INTERESTED IN

Nanofabricated solid immersion lenses registered to single emitters in diamond
Applied Physics Letters **98**, 133107 (2011); https://doi.org/10.1063/1.3573870

Monolithic diamond optics for single photon detection
Applied Physics Letters **97**, 241902 (2010); https://doi.org/10.1063/1.3519849

Microscopic diamond solid-immersion-lenses fabricated around single defect centers by focused ion beam milling
Review of Scientific Instruments **85**, 123703 (2014); https://doi.org/10.1063/1.4902818

AIP Publishing

Strongly enhanced photon collection from diamond defect centers under microfabricated integrated solid immersion lenses

J. P. Hadden,[a] J. P. Harrison, A. C. Stanley-Clarke, L. Marseglia, Y.-L. D. Ho, B. R. Patton, J. L. O'Brien, and J. G. Rarity
Centre for Quantum Photonics, Department of Electrical and Electronic Engineering & H. H. Wills Physics Laboratory, University of Bristol, Merchant Venturers Building, Woodland Road, Bristol BS8 1UB, United Kingdom

The efficiency of photon collection from optically active defect centers in bulk diamond is greatly reduced by refraction at the diamond-air interface. We report on the fabrication and measurement of a geometrical solution to the problem; integrated solid immersion lenses (SILs) etched directly into the surface of diamond. An increase of a factor of 10 was observed in the saturated count-rate from a single negatively charged nitrogen-vacancy (NV$^-$) within a 5 μm diameter SIL compared with NV$^-$'s under a planar surface in the same crystal. Such a system is potentially scalable and easily adaptable to other defect centers in bulk diamond. © *2010 American Institute of Physics.* [doi:10.1063/1.3519847]

The ability to address single defect centers in diamond using confocal microscopy allows optical access to these single "atom like" systems trapped within a macroscale solid. The negatively charged nitrogen-vacancy center (NV$^-$) is of particular interest for applications such as single photon generation,[1,2] nanoscale magnetometery,[3] and fundamental investigations of spin interactions and entanglement at cryogenic and room temperatures.[4–8] Other defect centers that exhibit single photon emission have been identified (e.g., the nickel-related "NE8,"[9] silicon-vacancy,[10] and chromium related centers[11]), but the search continues for other defect centers with spin properties like those of the NV$^-$ center.[12] The high refractive index of diamond causes refraction of the emitted light at the diamond-air interface, reducing the possible angular collection of a microscope objective. Thus, the NV$^-$ photon collection efficiency is severely reduced. This is a problem regardless of the application, or the particular defect center of interest. Here we report on the fabrication and measurement of hemispherical integrated solid immersion lenses (SILs) etched directly into the diamond surface. These structures eliminate surface refraction, thus increasing the numerical aperture (NA) of the microscope system. This allows a substantial increase in NV$^-$ photon collection efficiency along with improved background rejection. Moreover, this geometrical solution is potentially scalable and can easily be applied to other defect centers in bulk diamond.

The photon collection efficiency from NV$^-$ centers in diamond has previously been improved by using NV$^-$ centers located within nanocrystals small enough that the centers effectively emit into free space,[2,13] or nanophotonic structures such as nanowires which guide emission toward collection.[14] Photon collection is increased by a factor of up to about 5 in the former case and 10 in the latter. However, with the NV$^-$ centers positioned so close to the surface, local strain, impurities, and other surface effects have been shown to degrade the stability, and spin coherence time of the NV$^-$ center,[15,16] so a solution which improves the photon collection efficiency from NV$^-$ centers in bulk diamond is desir-

able. By etching hemispherical SILs into the surface of the diamond, we can increase photon collection efficiency without requiring the center to be close to the surface. Rays traced from a defect center located at the centroid of a sphere defining the SIL (hereafter termed as the centroid of the SIL) are normal to the surface at all points on the SIL. Therefore, no refraction occurs and the NA of collection is increased by a value equal to the refractive index ($n_d = 2.42$) of diamond.[17] This allows a significant increase in the collection efficiency.

Millimeter scale SILs placed on the surface of the sample have previously been used to boost photon collection from quantum dots[18,19] and single molecules in anthracene crystals.[20] However, these incur losses and aberrations caused by SIL-sample mismatch, surface reflections and gaps between the surfaces. The use of a microscale integrated SIL overcomes these problems, and is more scalable. Integrated microlenses have previously been fabricated in diamond using inductively coupled plasma etching (and other etching techniques), however they have not been used to improve collection of defect center emission.[21]

Using a finite-difference time-domain (FDTD) method, we simulated the collection efficiency (into a microscope objective with 0.9 NA) for a dipole located 2.5 μm below a planar diamond surface, at the centroid of a 2.5 μm radius SIL, and at the centroid of a 2.5 μm radius SIL surrounded by a 2.66 μm wide trench. The latter case is included because to etch the entire surface of the sample to the base of the SIL, as in the ideal case, would be too time consuming. The size of the trench is chosen such that the entire numerical aperture of the collection lens is utilized. It can be clearly seen from a cross-section of the simulated electromagnetic field intensity shown in Fig. 1(a)–1(c) that the SIL increases the field intensity crossing the diamond-air interface.

The collection efficiencies were calculated for wavelengths in the range of 600–800 nm (covering the majority of the NV$^-$ emission spectrum) and then an average was taken. The collection efficiencies calculated in this way were 5.6%, 29.8%, and 28.6%, respectively. The first two cases are consistent with efficiencies calculated by purely analytic methods.[22] In other words, we expect an ~5-fold increase in

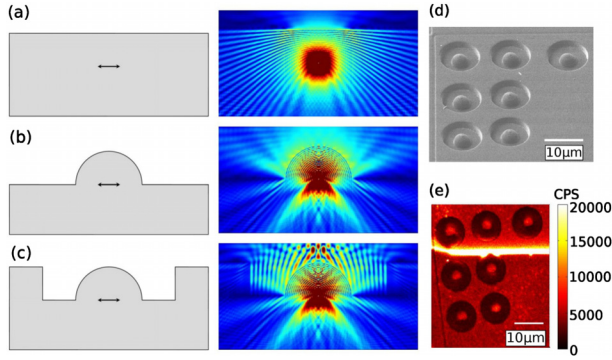[a]Electronic mail: jp.hadden@bristol.ac.uk.

FIG. 1. (Color online) Representation of electromagnetic field intensity in the YZ plane for a single frequency calculated from FDTD simulations for (a) a dipole 2.5 μm beneath a planar diamond surface, (b) a dipole at centroid of 2.5 μm radius SIL, and (c) a dipole at centroid of 2.5 μm radius SIL with 2.66 μm wide trench.(d) FIB image showing seven SILs and location grid lines. (e) Confocal image of the same area. The bright line is a diamond crystal grain boundary.
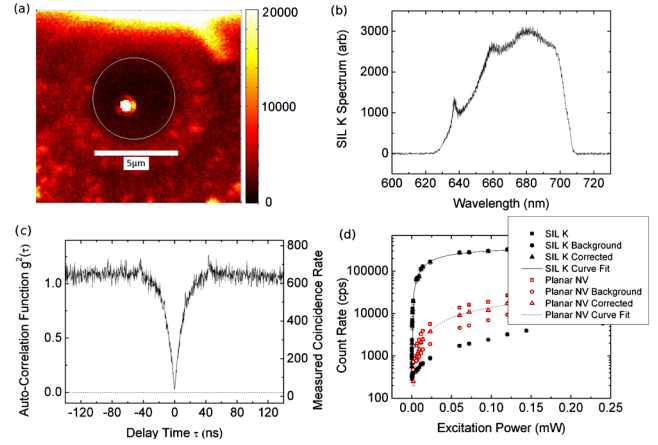

FIG. 2. (Color online) (a) Confocal image of SIL K. The boundary of the SIL is marked in white. Note that the color scale has been chosen to maximize the visibility of the SIL and the surroundings—the intensity of the bright spot is about 120 kc/s. (b) Optical spectrum recorded at the point of highest intensity in (a). The sharp drops in spectral intensity at 630 and 700 nm are caused by the spectral filter and not by chromatism in the SIL. (c) Second order intensity correlation function recorded at the same point as in (b). (d) Comparison of the total count-rate for the single NV$^-$ under SIL K with that for a single NV$^-$ under a planar surface as a function of excitation power. Filled (unfilled) symbols represent results from an NV$^-$ under a SIL (Planor surface). Squares represent the raw count-rate from the NV$^-$ center; circles represent the background rate measured from a point close to the NV$^-$ center. Triangles represent the net count-rate from the NV$^-$ center.

collection efficiency from geometrical considerations alone. However, it should be noted that in the planar case the effect of spherical aberration, which is significant for diamond material, is not included in the FDTD simulations or the analytic model. Spherical aberrations are eliminated in the hemispherical SIL geometry; therefore, we expect the measured enhancement in photon collection efficiency to be greater than 5.

The FDTD simulations also allow us to investigate the performance of the SILs when the dipole is not located precisely at the centroid of the SIL. Simulations show that if the dipole position is varied by 1 μm along any of the three Cartesian axes, the collection efficiency should remain above ~20% (cf. 28.6% at the centroid). In other words, the SILs are relatively tolerant to lateral or longitudinal placement error. It should also be noted that the SILs give an imaging magnification by factor of $n_{(d)}$ laterally, which means that a 1 μm lateral displacement in the diamond corresponds to a measured "image" distance in a confocal scan of 2.42 μm, placing it at the edge of the lens in a confocal image.[17]

SILs were fabricated in a polycrystalline type IIa chemical-vapor deposition diamond sample (Element Six) measuring ~5 mm×5 mm and of 1 mm thickness. There is a large variation in the density of NV$^-$ centers in the sample, and a region was chosen where the density was low enough to resolve single NV$^-$'s. A 30 keV gallium focused ion beam system (FEI Strata FIB-201) was used to fabricate the SILs. Hemispheres were approximated by etching concentric rings of increasing depth and diameter. This was achieved by varying the beam current and dwell time and water was used throughout to assist the etching process. A focused ion beam (FIB) image showing 7 of the 14 SILs fabricated along with FIB etched grid lines is shown in Fig. 1(d), and a confocal image of the same area is shown in Fig. 1(e).

Optical characterization was performed using a laser scanning confocal microscope system built in-house. The output from a frequency-doubled Nd:yttrium aluminum garnet laser (Cobolt Samba) was focused onto the sample using a 0.9 NA microscope objective (Nikon). Laser-induced fluorescence was collected by the same objective and focused onto the 8.9 μm core of an optical fiber (serving as the confocal aperture). A 532 nm long-pass filter was used to reject stray laser light. A band-pass filter centered at 675 nm

with a 67 nm transmission band was used to block the first and second order Raman scatter. It was tilted to shift the transmission band to 630–700 nm so that the NV$^-$ zero-phonon emission at 637 nm was transmitted. The fluorescence photons were then directed either to a spectrograph (Shamrock 303) fitted with a charge coupled device camera (Newton 920) to record optical spectra, or to a Hanbury-Brown and Twiss detection scheme to record the second order intensity correlation function $[g^{(2)}(\tau)]$.

Of the 14 SILs etched, 2 fell on grain boundaries and were not investigated further. Of the remaining 12, 5 contained single NV$^-$ centers. One of these 5 actually had two centers that could be resolved and analyzed separately. Only the data from the "best" of the single NV$^-$ containing SILs (denoted as "SIL K") are presented in full here.

A confocal scan of a 20×20 μm^2 area of the sample in the region of SIL K is shown in Fig. 2(a). A high intensity region is evident near the centroid of the SIL. This region is 1 μm away from the SIL's centroid in the confocal scan, corresponding to 0.41 μm in "real" space. The bright feature at the top is a grain boundary.

The optical spectrum recorded at this point [Fig. 2(b)] displays the characteristic NV$^-$ emission profile, with zero-phonon line around 637 nm and broad phonon assisted sideband at longer wavelengths. The antibunching dip in the second order intensity correlation function [Fig. 2(c)] clearly indicates that the emission arises from a single center. The data have been normalized and corrected for background as described by Beveratos *et al.*[2]

To quantify any enhancement in collection efficiency, the photon count-rate as a function of laser power was recorded for the NV$^-$ in SIL K and for other single NV$^-$ centers in the same diamond grain under an unmodified planar surface. A comparison of the saturated intensities [Fig. 2(d)] indicates an enhancement of ~10, with a measured absolute

count-rate of 345 kc/s. It should be noted that the absolute count-rate in our system could be improved by optimizing the spectral filters. By filtering between 630 and 700 nm, around 70% of the NV⁻ spectrum is being collected. In principle then, optimization of the filters would result in an absolute count-rate of 500 kc/s.

The three other SILs containing a single NV⁻ center had enhancement factors of 10, 8, and 8. For the SIL with two separate single NV⁻'s, the enhancement factors were 6 and 3.6.

As well as improving the angular collection efficiency, SILs also modify the profile of the confocal microscope's point spread function (PSF). Elimination of refraction in the excitation beam means that it can be focused to a smaller volume. Similarly, the volume imaged by the confocal pinhole is reduced. The cross-section of the PSF under a planor surface was estimated to be 360 ± 30 nm, compared with 120 ± 1 nm inside the SIL.[23] A reduction in size of the PSF is important because it decreases the proportion of unwanted background fluorescence collected along with the desired NV⁻ fluorescence. This is clearly visible in Fig. 2(d) where the signal to background ratio is much higher with the SIL, and in fact the absolute value of the background is three times lower at equivalent pump powers. A smaller excitation volume also means that the power density is increased for a given laser power and less power is required to saturate an NV⁻ center. SIL K obviously contains a very well positioned NV⁻center and we do see a variation in these enhancements from SIL to SIL. We ascribe this not only to NV⁻ position, and the SIL's fabrication quality, but also to variation of dipole orientation, since the crystal orientation is unknown in this polycrystalline sample. We are currently studying these effects.

This demonstration of strongly enhanced photon collection efficiency from NV⁻ centers using integrated solid immersion lenses is a step toward efficient single photon sources as well as efficient optical spin read-out in compact microstructured devices. The enhancement compares favorably to those reported from nanocrystal and nanowire devices,[13,14] with the advantage that NV⁻ centers are not located close to the surface where they might suffer from surface-induced decoherence. Since the enhancement is wavelength independent when the dipole is at the centroid of the SIL, it may be used with other defect centers in bulk diamond. Such a solution is robust and potentially scalable, since SILs could be fabricated over existing defect centers after characterization. Refinements in surface symmetry, SIL placement, and smoothness should enable greater enhancement as our fabrication technique is perfected.

[1]C. Kurtsiefer, S. Mayer, P. Zarda, and H. Weinfurter, Phys. Rev. Lett. **85**, 290 (2000).

[2]A. Beveratos, S. Kühn, R. Brouri, T. Gacoin, J.-P. Poizat, and P. Grangier, Eur. Phys. J. D **18**, 191 (2002).

[3]G. Balasubramanian, I. Y. Chan, R. Kolesov, M. Al-Hmoud, J. Tisler, C. Shin, C. Kim, A. Wojcik, P. R. Hemmer, A. Krueger, T. Hanke, A. Leitenstorfer, R. Bratschitsch, F. Jelezko, and J. Wrachtrup, Nature (London) **455**, 648 (2008).

[4]F. Jelezko, T. Gaebel, I. Popa, M. Domhan, A. Gruber, and J. Wrachtrup, Phys. Rev. Lett. **93**, 130501 (2004).

[5]R. Hanson, F. M. Mendoza, R. J. Epstein, and D. D. Awschalom, Phys. Rev. Lett. **97**, 087601 (2006).

[6]P. Neumann, N. Mizuochi, F. Rempp, P. Hemmer, H. Watanabe, S. Yamasaki, V. Jacques, T. Gaebel, F. Jelezko, and J. Wrachtrup, Science **320**, 1326 (2008).

[7]P. Neumann, J. Beck, M. Steiner, F. Rempp, H. Fedder, P. R. Hemmer, J. Wrachtrup, and F. Jelezko, Science **329**, 542 (2010).

[8]E. Togan, Y. Chu, A. S. Trifonov, L. Jiang, J. Maze, L. Childress, M. V. G. Dutt, A. S. Sørensen, P. R. Hemmer, A. S. Zibrov, and M. D. Lukin, Nature (London) **466**, 730 (2010).

[9]T. Gaebel, I. Popa, A. Gruber, M. Domhan, F. Jelezko, and J. Wrachtrup, New J. Phys. **6**, 98 (2004).

[10]C. Wang, C. Kurtsiefer, H. Weinfurter, and B. Burchard, J. Phys. B **39**, 37 (2006).

[11]I. Aharonovich, S. Castelletto, D. A. Simpson, A. D. Greentree, and S. Prawer, Phys. Rev. A **81**, 043813 (2010).

[12]J. R. Weber, W. F. Koehl, J. B. Varley, A. Janotti, B. B. Buckley, C. G. Van De Walle, and D. D. Awschalom, Proc. Natl. Acad. Sci. U.S.A. **107**, 8513 (2010).

[13]E. Ampem-Lassen, D. A. Simpson, B. C. Gibson, S. Trpkovski, F. M. Hossain, S. T. Huntington, K. Ganesan, L. C. Hollenberg, and S. Prawer, Opt. Express **17**, 11287 (2009).

[14]T. M. Babinec, B. J. M. Hausmann, M. Khan, Y. Zhang, J. R. Maze, P. R. Hemmer, and M. Loncar, Nat. Nanotechnol. **5**, 195 (2010).

[15]C. Bradac, T. Gaebel, N. Naidoo, M. J. Sellars, J. Twamley, L. J. Brown, A. S. Barnard, T. Plakhotnik, A. V. Zvyagin, and J. R. Rabeau, Nat. Nanotechnol. **5**, 345 (2010).

[16]J. R. Rabeau, A. Stacey, A. Rabeau, S. Prawer, F. Jelezko, I. Mirza, and J. Wrachtrup, Nano Lett. **7**, 3433 (2007).

[17]T. R. Corle and G. S. Kino, *Confocal Scanning Optical Microscopy and Related Imaging Systems* (Academic, San Diego, 1996).

[18]V. Zwiller, H. Blom, P. Jonsson, N. Panev, S. Jeppesen, T. Tsegaye, E. Goobar, M.-E. Pistol, L. Samuelson, and G. Bjork, Appl. Phys. Lett. **78**, 2476 (2001).

[19]Z. Liu, B. B. Goldberg, S. B. Ippolito, A. N. Vamivakas, M. S. Ünlü, and R. Mirin, Appl. Phys. Lett. **87**, 071905 (2005).

[20]J.-B. Trebbia, H. Ruf, P. Tamarat, and B. Lounis, Opt. Express **17**, 23986 (2009).

[21]C. Lee, E. Gu, M. Dawson, I. Friel, and G. Scarsbrook, Diamond Relat. Mater. **17**, 1292 (2008).

[22]W. Barnes, G. Björk, J. Gérard, P. Jonsson, J. Wasey, P. Worthing, and V. Zwiller, Eur. Phys. J. D **18**, 197 (2002).

[23]See supplementary material at http://dx.doi.org/10.1063/1.3519847 for details on estimation of the point spread function.